Magnetoresistance in Hybrid Organic Spin Valves at the Onset of Multiple-Step Tunneling

J. J. H. M. Schoonus, P. G. E. Lumens, W. Wagemans, J. T. Kohlhepp, P. A. Bobbert, H. J. M. Swagten, and B. Koopmans

Department of Applied Physics, cNM, Eindhoven University of Technology, The Netherlands

(Received 28 April 2009; published 2 October 2009)

By combining experiments with simple model calculations, we obtain new insight in spin transport through hybrid, CoFeB/Al_2O_3(1.5 nm)/tris(8-hydroxyquinoline)aluminium (Alq_3)/Co spin valves. We have measured the characteristic changes in the *I-V* behavior as well as the intrinsic loss of magnetoresistance at the onset of multiple-step tunneling. In the regime of multiple-step tunneling, under the condition of low hopping rates, spin precession in the presence of hyperfine coupling is conjectured to be the relevant source of spin relaxation. A quantitative analysis leads to the prediction of a symmetric magnetoresistance around zero magnetic field in addition to the hysteretic magnetoresistance curves, which are indeed observed in our experiments.

DOI: 10.1103/PhysRevLett.103.146601 PACS numbers: 72.25.Dc, 72.25.Rb, 72.80.Le, 85.75.−d

Organic semiconductors hold exceptional promise for spintronics [1,2]. Spin-polarized tunneling through an ultrathin (0–4 nm) Alq_3 layer [3] and spin transport in LSMO/Alq_3 (>30 nm) based devices [4,5] have been reported, thereby considerably stimulating the interest in organic spin valves [6–12]. However, spin injection and transport in an organic semiconductor are widely debated and similar results could also be interpreted within the classical tunneling concept [7,8,10]. Therefore, planar-type spin valves [4,9] and spin valves with insulating tunnel barriers [12] have been investigated to exclude tunneling transport via interdiffused clusters. Recently, direct observation of injected spin-polarized carriers inside the organic film have been reported [13,14]. Nevertheless, there still is a lack of consensus about the role of defect states [15], and little is known about the spin relaxation mechanisms.

Because of the insignificant spin-orbit spin relaxation, and since the time in between two successive hops could be relatively long (often >10 ns [16]), the electron spin on a localized molecular site can become particularly sensitive to small magnetic fields, for instance the randomly oriented local hyperfine fields from the hydrogen nuclei, $\vec{H}_{\mathrm{hf}}$ (Fig. 1) [17,18]. Devices exhibiting spin transport via one or a few hops in an organic semiconductor could provide a playground, which is complex enough to display all features related to the electron spin spending a finite time at molecular sites, but on the other hand simple enough to be treatable by analytical models.

In this Letter, we discuss how hyperfine fields can influence the spin injection and spin transport in organic semiconductors. Using a spin valve with a compound barrier, we have identified the transition regime between direct tunneling through the compound barrier and two-step tunneling via a low density of localized, intermediate (molecular or defect) states near the Fermi level. Only in the latter case hyperfine field coupling plays a significant role. In that regime, we will show that the experimentally observed modification of the hysteretic magnetoresistance curve is in line with model calculations including spin precession in the presence of hyperfine coupling.

Before we examine the detailed magnetic field dependence of the resistance, we first introduce a basic model that describes the competition between direct and two-step tunneling to derive the characteristic change in the resistance as a function of the Alq_3 thickness [Fig. 2(a)]. We consider an Alq_3 layer with a thickness d, a barrier height U, and a homogeneous distribution of molecular sites with linear density N, contacted on both sides by a ferromagnetic (FM) electrode. The extinction of the wave function in the Alq_3 layer is then defined as $\kappa = 2\sqrt{2mU}/\hbar$. d_1 and n_1 are the position and the occupation, respectively, of an intermediate site in the barrier. First, we assume only forward hopping. The direct tunneling current J_{direct} is proportional to $\exp[-\kappa d]$. The two-step tunneling current $J_{\mathrm{two\text{-}step}}$ follows from current conservation at the intermediate site, $J_{01} = J_{12}$, and subsequent solving n_1 from $(1 - n_1)\exp[-\kappa d_1] = n_1 \exp[-\kappa(d - d_1)]$.

In Fig. 2(c) the normalized $J_{\mathrm{two\text{-}step}}$ has been plotted for all possible d_1. The dominant contribution to the two-step tunneling current will be, by means of self-selection, via sites halfway the barrier with $d_1 \approx d/2$, for which the total transmission is maximum. The total current is proportional to a weighted superposition of direct tunneling and two-

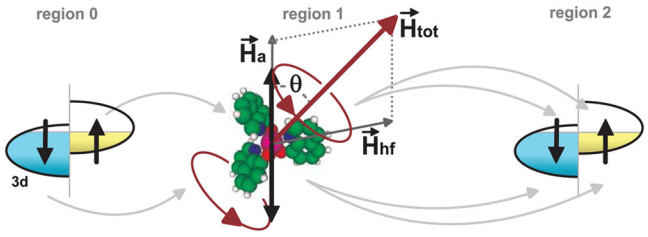

FIG. 1 (color online). Spin precession around the sum of the hyperfine field $\vec{H}_{\mathrm{hf}}$ and the applied magnetic field $\vec{H}_a$ on a molecular site, only showing downstream tunneling from or to majority and minority 3*d* spin bands of the FM electrodes.

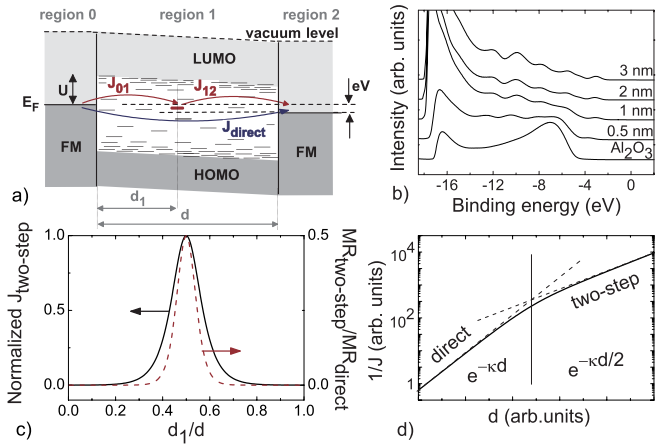

FIG. 2 (color online). (a) Schematic band diagram of Alq_3 in between two FM electrodes. (b) Valence band spectra for an increasing Alq_3 layer on Al_2O_3, see characteristic HOMO levels for 3 nm Alq_3. Calculation of (c) J and MR for two-step tunneling as a function of d_1, (d) $1/J$ as function of d.

step tunneling:

$$J \sim (1 - Nd)J_{\text{direct}} + N\int_0^d J_{\text{two-step}}(d_1)dd_1. \qquad (1)$$

With increasing d, two-step tunneling is favorable. Because both transmissions of the two-step tunneling process are proportional to $\exp[-\kappa d/2]$, the total resistance ($\sim 1/J$) will increase exponentially with half the slope of the regime of direct tunneling [Fig. 2(d)]. Thereby, we can identify the onset of two-step tunneling.

Ta/CoFeB/Al_2O_3/Alq_3/Co spin valves were fabricated completely *in situ* at base pressures $<1 \times 10^{-8}$ mbar on glass substrates via shadow masks in a cross bar configuration, defining a junction area of 0.3×0.3 mm^2. Al_2O_3 enhances the growth characteristics of Alq_3 and improves the spin injection and detection efficiency [3]. On a Ta(2 nm)/CoFeB(2 nm) bottom electrode Al(1.2 nm) is deposited by dc magnetron sputtering and is subsequently plasma oxidized. Alq_3 ($d_{Alq_3} = 0$–4 nm) is evaporated from a Knudsen cell at a rate of $\sim$0.04 Å/s keeping a substrate temperature of 110 K. Finally, a Co top electrode of about 20 nm thickness is evaporated, and the whole sample is capped by 5 nm SiO_2. The valence band spectra for increasing Alq_3 thicknesses deposited on Al/Al_2O_3 [see Fig. 2(b)] as well as on Co (not shown) surfaces have been measured with ultraviolet photoemission spectroscopy. Results show a disappearance of the Al_2O_3 valence band between 1.0 and 1.5 nm, indicating that a closed layer of Alq_3 has been obtained, although a small density of pinholes cannot be completely excluded via this technique.

To be able to identify when two-step tunneling dominates over direct tunneling, we have measured the *I-V* characteristics with a four-point probe technique at various temperatures and d_{Alq_3}. All dI/dV are parabolic and slightly asymmetric (not shown), which suggests tunneling as transport mechanism. In Fig. 3 (open circles), the resistances of all spin valves showing magnetoresistance (yield of $\sim$40%) have been plotted as a function of d_{Alq_3}. For $d_{Alq_3} = 2$–4 nm, the exponential increase of resistance levels off, which we assign to the predicted transition to the regime of two-step tunneling. Upon cooling to 4 K the conductance decreases to 60% of the conductance at 300 K (not shown). This generally rules out that charge transport through metallic filaments or via pinholes is dominant [7].

Subsequently, the magnetic field dependence of the spin-valve resistance has been measured for different d_{Alq_3}. First, we will analyze the magnetoresistance (MR), defined by $(R_{ap}/R_p - 1) \times 100\%$, as a function of d_{Alq_3} (Fig. 3, solid squares). $R_{p(ap)}$ is the spin-valve resistance for (anti-) parallel magnetization alignment. Already for 1 nm, still in the regime of direct tunneling, the MR significantly reduces compared to a measured MR of 34% for a single Al_2O_3 barrier. After the onset of two-step tunneling, for $d_{Alq_3} \geq 2$ nm, the MR decreases even further. We note that none of those devices with more than 1 nm Alq_3 shows a MR larger than 10%, which is in line with organic spin valves with Co, Fe, or Ni electrodes [3,11].

To obtain a quantitative interpretation of the resistance and MR as a function of d_{Alq_3}, we extend our model. (i) We include the spin dependence of the electrons. Therefore, we replace n_1 by $n_{1\uparrow}$ and $n_{1\downarrow}$ and take into account the normalized spin occupancy in the FM electrodes $(1 \pm P_0)/2$ and $(1 \pm \alpha P_2)/2$, with P_0 and P_2 the spin polarization of the injection and detection electrode, respectively, and $\alpha = (-)1$ for (anti-)parallel magnetization alignment. (ii) We add an Al_2O_3 layer with thickness $d_{Al_2O_3}$ and barrier height $U_{Al_2O_3}$. (iii) Because the energy penalty is modest [16], we allow double occupancy of a site by electrons with opposite spin directions. (iv) Since our aim is to solve the tunnel rates in the low bias, Ohmic regime, we permit back hopping by a rate according to the Fermi-Dirac distribution.

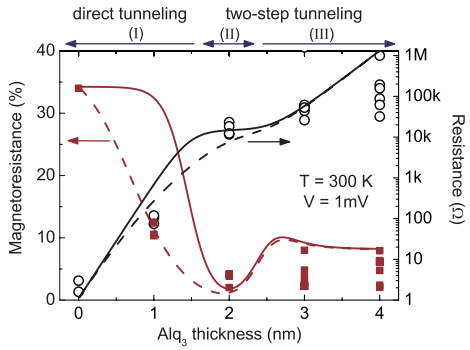

FIG. 3 (color online). Room-temperature resistance (circles, right axis) and MR (squares, left axis) for variable Alq_3 thicknesses. Lines are fits based on model (solid lines: basic model, dashed lines: with hybridization at Alq_3/Co interface).

With these refinements, the total resistance [$\sim 1/J$ from Eq. (1)] has been calculated for reasonable parameters ($U_{Al_2O_3} = 2.5$ eV, $U_{Alq_3} = 0.4$ eV, and $d_{Al_2O_3} = 1$ nm) [3], and is subsequently fitted to the experimental results (Fig. 3 solid line, using $N = 3 \times 10^{-5}$ Å^{-1}). Three regimes can be distinguished (Fig. 3, top axis): (I) For low d_{Alq_3}, direct tunneling dominates. (II) This regime is characterized by two-steps tunneling, and the transmission through the Al_2O_3 barrier is smaller than through the Alq_3 barrier. The largest current contribution comes from tunneling via a site near the Al_2O_3/Alq_3 interface, and the resistance will hardly change with d_{Alq_3}. (III) For large d_{Alq_3} two-step tunneling dominates and the total resistance will exponentially increase with half the slope of the first regime. Finally, for thicker organic layers the number of tunnel steps increases and the resistance will increase with an even lower slope.

Subsequently, using $P_0 = P_2 = 0.4$, the MR has been calculated and is plotted as a function of d_{Alq_3} (Fig. 3, solid line, normalized to MR [$d_{Alq_3} = 0$]). In the regime of direct tunneling (I), the modeled MR is unaltered. However, for two-step tunneling (regimes II and III), the model predicts that the MR reduces at least with a factor ≈ 4, which matches with the maximum experimentally found MR. The factor 4 can be explained as follows. Tunneling via an intermediate site results in an intrinsic loss of MR by a factor 2 [19]. Additionally, as can be seen in Fig. 2(c), the MR is highest for sites for which transmissions through both tunnel barriers are equal, i.e., because the dominant current contribution is also via these sites, the system self-optimizes its MR. Weighting the MR for the current contribution over all intermediate sites predicts an extra averaged loss of MR by approximately a factor 2. In regime II, the transmission through both tunnel barriers cannot be equal, predicting an extra MR loss.

The even lower measured MR can possibly be explained by refining the model by (i) including a strong hybridization at the Alq_3/Co interface that results in more interface sites, thereby forcing tunneling via sites with unequal transmission of both barriers (Fig. 3, dashed lines), (ii) permitting more than two tunnel steps, which may lead to a further decrease of MR, (iii) lowering of the spin polarization of Co adjacent to Alq_3, and (iv) including spin precession due to hyperfine coupling, thereby not reaching the maximum resistance for antiparallel magnetization alignment as explained below.

Let us now analyze in more detail the hysteretic magnetoresistance curves for devices with 1, 2, and 4 nm Alq_3 [Figs. 4(a)–4(c)], which are representative for the direct, the transition, and the two-step tunneling regime, respectively. The MOKE measurement in Fig. 4(d), performed on the spin valve with 4 nm Alq_3, displays nearly instantaneous switching of the magnetizations of both electrodes. These differences in coercivities yield parallel and antiparallel magnetization alignment, resulting in the low and high resistance states, respectively [Figs. 4(a)–4(c)]. For a device with $d_{Alq_3} \geq 2$ nm the magnetoresistance curve is modified with a symmetric positive (negative) contribution in the parallel (antiparallel) alignment. As we will explain later, it is difficult to interpret the symmetric contribution as originating from the magnetic states of the electrodes only, and we believe that the responsible mechanism is dominated by intrinsic transport processes.

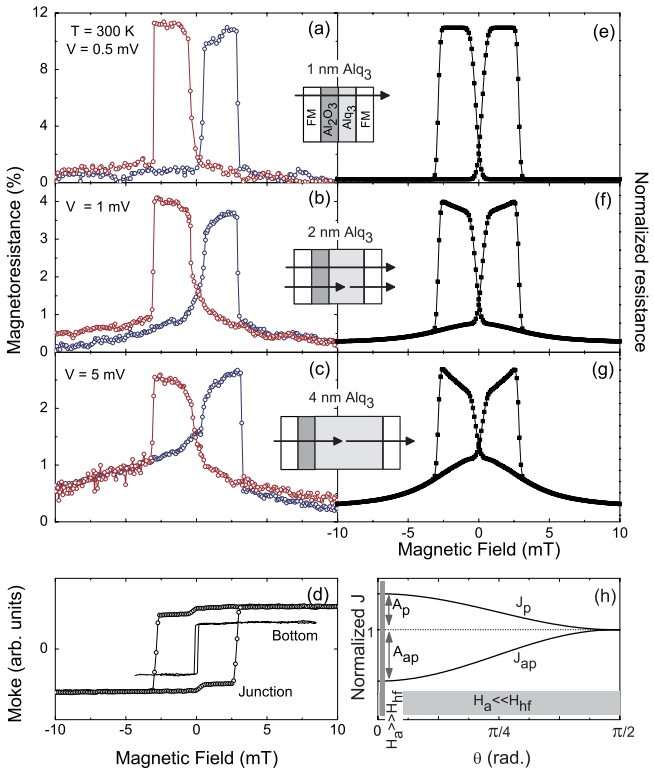

FIG. 4 (color online). Magnetic field dependencies for $CoFeB/Al_2O_3/Alq_3$ (1, 2, 4 nm)/Co spin valves (a)–(c) measured (e)–(g) modeled. (d) Magnetization curves of the junction and bottom electrode of the sample with 4 nm Alq_3. (h) Representative calculation of normalized current versus θ, with indications of applicable areas for large and small H_a.

By introducing spin precession at a molecular site, due to hyperfine coupling, we aim at understanding the measured magnetoresistance curves. We consider the situation that an electron, while preserving its spin, is injected from the FM electrode into a molecular site. While occupying the site, the electron spin couples via the exchange interaction and/or via a direct dipole-dipole interaction to a randomly orientated total hyperfine field $\vec{H}_{hf}$ of the local hydrogen nuclei, which can be assumed to be a three-dimensional Gaussian distribution with an average magnitude of a few mT's [16] (Fig. 1). The electron spin motion can be described as a coherent precession around the vector sum of the total hyperfine field and the external applied magnetic field, $\vec{H}_{tot} = \vec{H}_{hf} + \vec{H}_a$, canted at an angle θ with respect to the magnetization axis of the electrodes. We have calculated that for the dominant current contribution

[Figs. 2(c) and 3] the spin precession frequency around the total magnetic field, $g\frac{e}{2m}H_{\mathrm{tot}}$, is at least an order of magnitude larger than the tunnel rate $2\pi\exp[-\kappa d]/t_{\mathrm{at}}$. Herein, the Landé-factor $g \approx 2$ and the attempt time $t_{\mathrm{at}} \approx 1$ fs. Thereby, we have experimentally fulfilled the necessary precondition to use a time averaged projection operator $\mathbf{M}_{\pm\pm}$, to describe the hopping probabilities from the precessing spinor states $\chi_{1\pm}(t)$, expressed in terms of spin-up and spin-down states, to the spinor states $\chi_{2\pm}$ in the detection electrode. Using these ingredients, we have again solved the tunnel rates like in our basic model approach. The normalized two-step tunneling current can be more generally expressed as $1 + A_{p(\mathrm{ap})}\cos(\theta)^2$, for which $A_{p(\mathrm{ap})}$ for parallel (antiparallel) magnetization alignment depends on the introduced parameters and further details of the implementation of the model [Fig. 4(h)].

For $d_{\mathrm{Alq_3}} = 1$ nm, the direct tunneling current dominates and is independent of $\mathbf{M}$ and thus θ. Thereby, the normalized magnetoresistance curve follows directly from the magnetization switchings as shown in Fig. 4(d) [Fig. 4(e)]. The magnetoresistance curve for 4 nm Alq_3, representing two-step tunneling, has been reconstructed using $A_p = 0.18$, $A_{\mathrm{ap}} = -0.20$, and 3 mT for the average magnitude of the Gaussian hyperfine field distribution [Fig. 4(g)]. The magnetoresistance curves can be interpreted as follows. For $H_a \gg H_{\mathrm{hf}}$, spins preserve their alignment with the external magnetic field [$\theta \approx 0$ in Fig. 4(h)] and the resistance difference between parallel and antiparallel alignment is expected to be similar to the case of direct tunneling. For $H_a \ll H_{\mathrm{hf}}$, each spin at a molecular site precesses around $\vec{H}_{\mathrm{hf}}$. Averaged over all occupied sites, these total sums of hyperfine fields will have a spherical distribution [$0 < \theta < 2\pi$ in Fig. 4(h)]. This results in an increased (decreased) resistance for parallel (antiparallel) magnetization alignment. For 2 nm Alq_3, the direct tunneling current approximately equals the two-step tunneling current as shown in Fig. 3, resulting in a weighted average of the magnetoresistance curves for 1 and 4 nm Alq_3 [Fig. 4(f)].

Several features predicted by the model are present in our experimental results [e.g., Figs. 4(c) and 4(g)], like the gradual and sharp resistance change accompanying the transition to and from parallel to antiparallel magnetization alignment of the electrodes. Second, the reproducible full width half maximum of the symmetric modification corresponds to a typical value for H_{hf} [17,20].

We have several reasons why we exclude a different interpretation for the symmetric contribution. First, we exclude that the effect originates from magnetic switching of the bottom CoFeB electrode, because this would lead to identical normalized magnetoresistance curves. Second, tunneling via regions in the top Co electrode with an altered easy axis is improbable, because this would give an opposite sign of the symmetric modification for antiparallel magnetization alignment. Third, if the symmetric modification would be the result of the resistance of the electrodes, of the Al_2O_3 barrier or of the interface, we would have observed a reduction of the symmetric contribution considering the tendency of increasing spin-valve resistance for increasing $d_{\mathrm{Alq_3}}$ (Fig. 3). Finally, we consider it unlikely that transport via sites next to paramagnetic clusters or via sites exposed to stray fields contributes to the symmetric contribution, because one would expect in this case a wide distribution of magnetic field scales, associated with the diversity of cluster sizes and the disordered landscape of protrusions at the Alq_3/Co interface.

In conclusion, by modeling the spin transport through Al_2O_3/Alq_3, we can explain the characteristic changes in the I-V behavior at the onset of multiple-step tunneling, as well as the intrinsic loss of MR. Furthermore, spin precession in the presence of hyperfine coupling has been analyzed, by which the measured magnetoresistance curves can be recovered for variable Alq_3 thickness.

This work was supported by the Dutch Technology Foundation (STW) via NWO VICI-grants "Spin Engineering in Molecular Devices" and "Spintronics."

[1] S. Sanvito, Nature Mater. **6**, 803 (2007).
[2] Z. V. Vardeny, Nature Mater. **8**, 91 (2009).
[3] T. S. Santos *et al.*, Phys. Rev. Lett. **98**, 016601 (2007).
[4] V. Dediu, M. Murgia, F. C. Matacotta, C. Taliani, and S. Barbanera, Solid State Commun. **122**, 181 (2002).
[5] Z. H. Xiong, D. Wu, Z. V. Vardeny, and J. Shi, Nature (London) **427**, 821 (2004).
[6] S. Majumdar *et al.*, Appl. Phys. Lett. **89**, 122114 (2006).
[7] W. Xu *et al.*, Appl. Phys. Lett. **90**, 072506 (2007).
[8] J. S. Jiang, J. E. Pearson, and S. D. Bader, Phys. Rev. B **77**, 035303 (2008).
[9] T. Ikegami *et al.*, Appl. Phys. Lett. **92**, 153304 (2008).
[10] H. Vinzelberg *et al.*, J. Appl. Phys. **103**, 093720 (2008).
[11] J. H. Shim *et al.*, Phys. Rev. Lett. **100**, 226603 (2008).
[12] Y. Q. Zhan *et al.*, Phys. Rev. B **78**, 045208 (2008).
[13] M. Cinchetti *et al.*, Nature Mater. **8**, 115 (2009).
[14] A. Drew *et al.*, Nature Mater. **8**, 109 (2009).
[15] S. Boukari *et al.*, Phys. Rev. B **76**, 033302 (2007).
[16] P. A. Bobbert *et al.*, Phys. Rev. Lett. **99**, 216801 (2007).
[17] K. Schulten and P. G. Wolynes, J. Chem. Phys. **68**, 3292 (1978).
[18] P. A. Bobbert *et al.*, Phys. Rev. Lett. **102**, 156604 (2009).
[19] A. Fert and H. Jaffrès, Phys. Rev. B **64**, 184420 (2001).
[20] F. Gerson and W. Huber, *Electron Spin Resonance Spectroscopy for Organic Radicals* (Wiley-VCH, Weinheim, 2003).